Surface & Coatings Technology 266 (2015) 160–166

Contents lists available at ScienceDirect

Surface & Coatings Technology

journal homepage: www.elsevier.com/locate/surfcoat

# Evaluation of antibacterial activity of anticorrosive electroless Ni–P coating against *Escherichia coli* and its enhancement by deposition of sono-synthesized ZnO nanoparticles

Zahra Sharifalhoseini [a], Mohammad H. Entezari [a,b,*], Razieh Jalal [c]

[a] Sonochemical Research Center, Department of Chemistry, Faculty of Science, Ferdowsi University of Mashhad, 91775 Mashhad, Iran
[b] Environmental Chemistry Research Center, Department of Chemistry, Faculty of Science, Ferdowsi University of Mashhad 91775, Mashhad, Iran
[c] Biochemical Research Center, Department of Chemistry, Faculty of Science, Ferdowsi University of Mashhad, 91775 Mashhad, Iran

ARTICLE INFO

*Article history:*
Received 14 December 2014
Accepted in revised form 16 February 2015
Available online 24 February 2015

*Keywords:*
Metallic surface
Sonosynthesized ZnO NPs
Antibacterial surface

ABSTRACT

The adhesion and proliferation of bacteria on metallic surfaces in different places such as health centers, industries and even homes increase the risk of human infections. In the present research, mild steel as a substrate was coated with a Ni–P layer through electroless plating to prevent surface corrosion of the steel. In order to achieve an antibacterial metallic surface, simultaneous sono-synthesis and deposition of ZnO nanoparticles (NPs) were performed on this Ni–P coating. The morphology and chemical composition of the ZnO coated plate were characterized by the use of scanning electron microscopy (SEM) and energy-dispersive X-ray spectroscopy (EDX). The X-ray diffraction (XRD) pattern confirmed that the ZnO was pure and showed a hexagonal structure. The antibacterial activity assay of the electroless Ni–P coating against *Escherichia coli* O157:H7 showed some biological activity but the plate containing ZnO NPs effectively prohibited the growth of *E. coli*. It is concluded that the attached ZnO surface could be utilized for antibacterial purposes by reduction of colonization.


## 1. Introduction

Significant progress in technology and the growth in industry have led to improvements in human life. On the other hand, the production of pollutants has increased and their entry into the environment has resulted in the rapid growth of microbes. This phenomenon can perturb the natural balance of various kinds of microorganisms in the environment. Uncontrolled growth of microorganisms creates serious problems such as spreading of various infections is risking human health [1]. Health-care-associated infection is one of the ten major reasons of death in the United States. The report of the Center for Disease Control (CDC) claims that 99,000 deaths occur in the USA annually due to 1.7 million infections [2]. Utilization of antibacterial agents is necessary to prevent or reduce the microorganism growth and their harmful effects in our life. Since the spreading of infections is highly probable in health care centers, development of antibacterial surfaces can help to provide a sterile environment in these places. Several different groups work on the production of antimicrobial surfaces. For instance, the generation of antimicrobial textiles used for the medical applications in hospitals and other places where the presence of bacteria is a major hazard [3–6]. Glass coated with ZnO NPs as a rigid antibacterial matrix [7], antibacterial paper [8–10], and polyethylene film deposited by ZnO NPs [11,12], are other examples of the antibacterial surfaces.

Despite the wide range of successful attempts on the production of antibacterial surfaces including different types of textiles, papers and even glasses, metallic surfaces have been less well studied. It should be mentioned that bacterial colonization after the attachment of viable bacteria on metallic surfaces and interfaces leads to biofilm formation. Apart from hospital-acquired infections which are attributed to bacteria growth on medical devices and implants, the presence of thin biofilms on other general surfaces results in harmful effects on the environment. From this perspective the goal is to develop general metallic structures that could be utilized to inhibit or reduce the bacterial growth. Therefore, in this work, steel alloy has been chosen as substrate due to its extensive applications in metal fasteners, doors, beds and other metal constructions. This antibacterial metallic surface could be useful for inhibition or reduction of the bacterial colonization in every place where the presence and the thriving of bacteria are highly probable.

In these experiments, the method of sonication due to its advantages has been applied to the ZnO deposition. Ultrasonic waves cause creation of the cavities in the solution, the collapse of these cavities produces shockwaves which lead to an increase of mass transfer. Furthermore, asymmetric collapse near the surface in a heterogeneous medium

* Corresponding author at: Sonochemical Research Center, Environmental Chemistry Research Center, Department of Chemistry, Faculty of Science, Ferdowsi University of Mashhad, 91775 Mashhad, Iran. Fax: +98 511 8795457.
*E-mail address:* moh_entezari@yahoo.com (M.H. Entezari).

http://dx.doi.org/10.1016/j.surfcoat.2015.02.035
0257-8972/

results in a microjet which sweeps the surface at high speed and causes the surface activation by the removal of any contaminant from the surface. These advantages make method of sonication highly appropriate for many practical applications such as improving the rates of chemical reaction with higher efficiency in comparison with classical methods [13,14].

ZnO was deposited on the surface for two practical purposes: the preparation of antibacterial surface and the enhancement of the anticorrosion performance of the Ni–P coating. It is known that ZnO in addition to inhibitory action against gram-positive and gram-negative bacteria, and even spores which are resistant to high-temperature and high-pressure [15,16], was found as a protective ceramic oxide. The last item makes it a valuable candidate for production of anticorrosive coatings [17–19]. The results of biological activity on this multifunctional platform surface have been investigated in the present work. Moreover the antibacterial action of electroless Ni–P coating against *Escherichia coli* has been reported in this paper too.

## 2. Experimental

### 2.1. Materials

All reagents including, nickel sulfate, $NiSO_4$ $(H_2O)_6$, sodium hypophosphite, $NaPO_2H_2$, trisodium citrate, $Na_3C_6H_5O_7$, sodium dodecyl sulfate (SDS), zinc chloride, $ZnCl_2$, and potassium hydroxide, KOH were purchased from Merck and used without additional purification. Steel (Fe—99.340, Cu—0.043, Sn—0.001, Co—0.007, Al—0.059, Ni—0.031, Mo—0.001, Ti—0.001, P—0.013, S—0.033, Cr—0.028, C—0.024, Si—0.058, Mn—0.387-wt.%) was chosen as substrate.

### 2.2. Electroless Ni–P composite coating

The steel substrate was divided into plates of 20 mm × 20 mm × 1 mm which were then washed with acetone to clean the surface from any contaminants. Removal of oxide layer from the metal surface was carried out by the immersion of the plate in hydrochloric acid (HCl, 12 M) for 30 s, followed by rinsing with distilled water, the excess acid on the surface was neutralized by basic solution (NaOH, 1 M). The surface activation was done by soaking the sample in acidic solution (HCl, 0.1 M) for 2 min. Since the chosen substrate was the mild steel, its surface is highly susceptible to oxidation when exposed to air. Therefore, Ni–P layer was coated on the surface by the electroless method to improve corrosion resistance. The acid bath for electroless nickel plating was composed of nickel sulfate as $Ni^{2+}$ source, sodium hypophosphite as reducing agent and sodium citrate as complexing agent. A slight amount of sodium dodecyl sulfate (SDS) was also used in the same bath. Addition of SDS as a surfactant reduces the surface tension and leads to easy removal of hydrogen bubbles from the surface and results in a smooth and pit-free protective layer. During the coating process, the pH was adjusted at 4.8–5.0 and the temperature was kept at 80 °C. After 120 min of electroless nickel plating, the coated plate was drawn from the bath and rinsed with distilled water.

### 2.3. ZnO NPs deposition

First, 25 mL of aqueous solution (KOH, 1 M) was poured into a cell equipped with water jacket to keep the temperature at 80 °C, then the sample (Ni–P coated plate) was mounted with a Teflon holder under the sonicator horn. The optimum position of the sample was found to be 2 cm below the horn. Then 25 mL of an aqueous solution ($ZnCl_2$, 0.5 M) was added gently from a burette to the KOH solution. During the reaction, ultrasonic waves were emitted from the sonicator 20 kHz (XL 2020) for about 30 min. Fig. 1 shows a schematic view of the experimental set-up used in this part.

After simultaneous synthesis and deposition of ZnO, the plate was rinsed in distilled water and dried at 80 °C in an oven. The loose and unbound particles were removed from the surface by rubbing the resultant surface with a clean cloth. Then, the plate was used for characterization by SEM and EDX techniques.

### 2.4. Synthesis of ZnO NPs

To ensure the purity of the ZnO NPs which were synthesized by the procedure used in this research, the metal oxide was fabricated

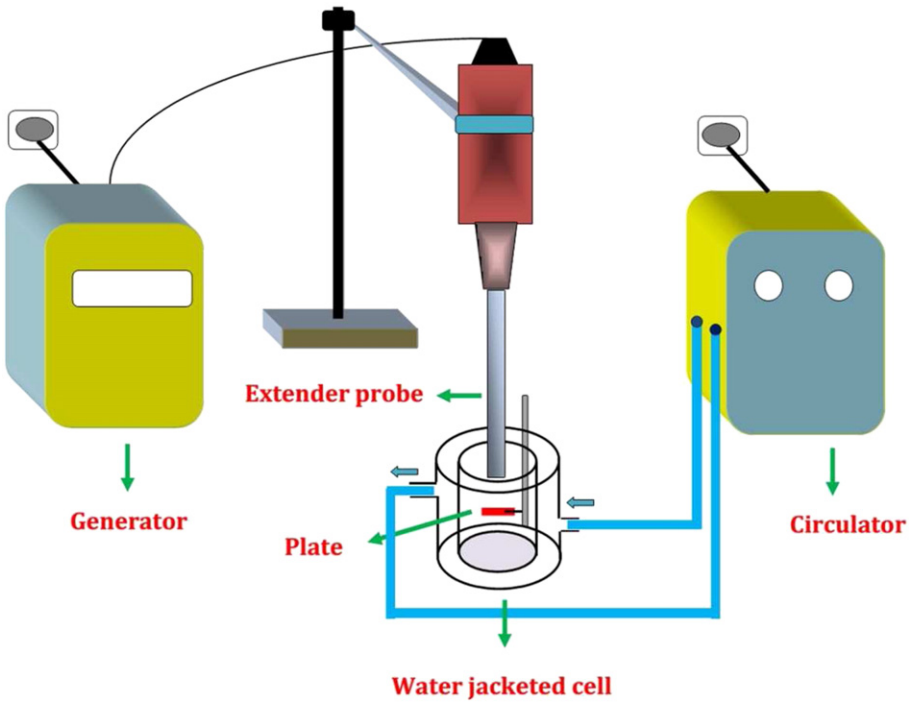


**Fig. 1.** Schematic view of the experimental set up.

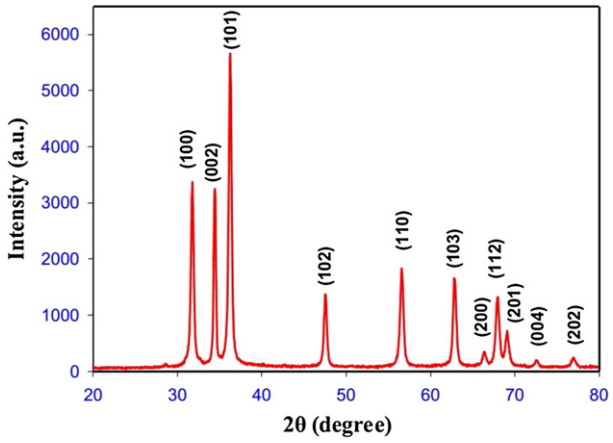


**Fig. 2.** XRD pattern of ZnO nanoparticles synthesized under ultrasound.

separately and characterized. The white powder of ZnO was synthesized in the same mentioned way (Section 2.3), but without the substrate. The powder was collected from the bottom of the cell and separated by centrifugation (rpm = 5000 for 5 min), washed with distilled water for several times, and then dried in oven at 80 °C for 18 h. The structure of the sample was characterized by XRD and its morphology determined by TEM.

### 2.5. Characterization

The crystallographic structure for ZnO powder was determined using X-ray diffractometer (D8 advanced) equipped with Cu Kα radiation (λ = 0.154 nm). The XRD pattern was collected within the 2θ range of 20 to 80 °C with a scanning rate 0.1° $s^{-1}$. Morphology of the resultant powder was studied by TEM (Philips BioTwin*CM120 TEM*). A small amount of powder was dispersed in ethanol by the focus of an ultrasonic bath for 20 min and then a droplet of suspension was added onto carbon-coated grids and the TEM micrographs were taken after evaporation of solvent. The surface of the alloy containing ZnO nanoparticles was monitored by microscope (LEO 1450 VP). Three dimensional micrographs of the surface were scanned by this instrument. The elemental composition of the surface was determined by EDX coupled to the SEM instrument.

### 2.6. Antibacterial activity test

#### 2.6.1. Colony count method

Gram-negative *E. coli* O157:H7 was grown overnight at 37 °C in tryptic soy broth (TSB). The saturated culture was diluted in fresh TSB medium and incubated at 37 °C for 3 h. Subsequently, the bacterial suspension was added into TSB medium with a final concentration of $10^5$ CFU $mL^{-1}$ (CFU: colony forming unit). Evaluation of the antibacterial activity was carried out by colony count method. For this test, in addition to the plate containing ZnO, another plate without ZnO was examined to exclude the effect of the Ni–P layer on antibacterial activity. To sterilize, the plates were autoclaved at 121 °C for 15 min, then the test samples were placed in wells of a 6-well plate individually and bacterial suspension ($10^5$ CFU $mL^{-1}$) was added. Then the final volume of each well was brought up to 3 mL with the addition of TSB. Positive and negative control groups were also cultured under the same conditions. Microbial suspension without the test sample was used as positive control and TSB media was considered as negative control. The plates were incubated at 37 °C on a reciprocal shaker. After 3 h, 100 μL of each sample was diluted appropriately in TSB and then it was plated onto the tryptic soy agar (TSA) plate. The number of colonies was counted after 24 h of incubation at 37 °C.

#### 2.6.2. Zone of inhibition test

The biological activity of the target plate was also examined by zone of inhibition test. For this experiment, 100 μL of the bacterial suspension ($10^4$–$10^5$) CFU $mL^{-1}$ was uniformly spread over the TSA agar plate and the sample was placed at the center of the petri dish. For this test, Ni–P coated plate was considered as the blank sample. The plates were incubated at 37 °C for 24 h. It should be mentioned that the use of the mild steel without the coating was not possible due to its corrosion in the moderate conditions of the experiment.

## 3. Results and discussion

### 3.1. XRD analysis of ZnO

Fig. 2 shows all diffraction peaks of ZnO which attributed to the planes including (1 0 0), (0 0 2), (1 0 1), (1 0 2), (1 1 0), (1 0 3), (2 0 0), (1 1 2), (2 0 1), (0 0 4), and (2 0 2).

The pattern was well matched with the standard data (JCPDS data card No. 89-1397). It is evident that the sample is pure. This pattern

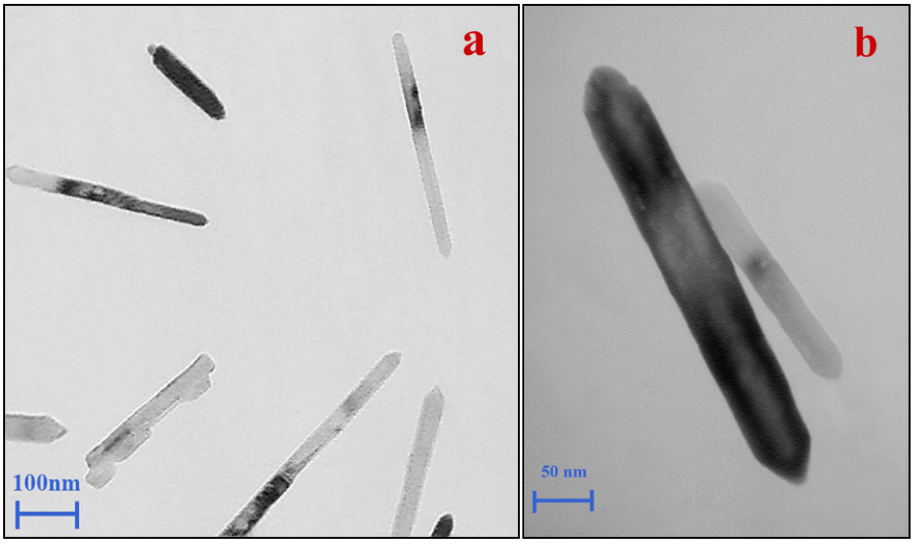


**Fig. 3.** TEM images of ZnO nanoparticles in a nanorod form synthesized by sonication. Figures (a) and (b) demonstrate the resultant product at low and high magnifications, respectively.

also implies hexagonal wurtzite phase with lattice constants of a = b = 3.242 Å and c = 5.205 Å.

### 3.2. ZnO NPs morphology

Fig. 3(a) and (b) shows the TEM images of ZnO NPs at two levels of magnification. It is evident that the obtained ZnO was crystallized in a hexagonal rod-like structure. The diameter of these ZnO nanorods was almost the same but they had unequal length. The length of the nanostructures was in the range of 100–300 nm and the diameter was about 20–30 nm.

### 3.3. Morphology of the ZnO deposited on the surface

To have a good picture of the morphology, 3D scanning of the surface was evaluated and represented at three different magnifications in Fig. 4(a–c). The low magnification (Fig. 4(a)) features a map projection in which the presence of peaks is attributed to the Ni–P phase. Observation of the ZnO nanostructures is perfectly clear at higher magnifications (Fig.s 4(b) and (c)). From these micrographs, the shapes of ZnO nanocrystals (NCs) are easily distinguishable.

As a result, while for the ZnO powder the nanorod structure was detected as the dominant form (Fig. 3(a) and (b)), in the presence of the rigid surface other shapes could be detected. It seems that the existence of the other shapes like the spherical and the flower-like structures was due to the presence of rigid substrate. The formation of the flower-like structures in the presence of ultrasound (shown by circles in Fig. 4(c)) could be illustrated by the cavitation process.

The asymmetric collapse of cavities near the surface generates microjets. The microjets and shockwaves produced by cavitation process lead to substantial changes on the surface of the solid phase present in the medium [20]. The harsh conditions during the cavitational collapse result in appropriate situation for the of joining the nuclei in the primary nucleation process. It means that the fusion in elementary nuclei can be attributed to the hot spots which assigned to explosion of cavities in the medium and specially microjets created near the surface. Fig. 5 shows a schematic illustration for this phenomenon. In addition of cavitation process, the precursors for the formation of ZnO are shown in this schematic too.

On the other hand, ultrasonic irradiation prevents ZnO nanoparticles from agglomerating and leads to uniform availability of the nanoparticles on the surface. Furthermore, effective collisions between products and the surface result in strict adherence to the surface. It is obvious from Fig. 4(c) that the formation of ZnO nanocrystals with approximate uniform distribution is due to the abovementioned ultrasonic effects. Note that the application of some additive materials such as capping agents can control the synthesis of distinct shapes. But, in this study the antibacterial surface was prepared in quick and easy way without any additives.

### 3.4. Energy-dispersive X-ray spectroscopy

The EDX analysis confirmed the presence of the expected elements including zinc, oxygen, nickel and phosphorus on the surface (Fig. 6). Weight percent of the defined area marked on this figure is shown in Fig. 6.

### 3.5. Antibacterial activity assay

Evaluation of antibacterial activity of the target plates was performed by using the colony count method. Fig. 7(a) shows the exposure of the samples to the bacterial suspension ($10^5$ CFU $mL^{-1}$) in wells of a 6-well plate. The viable *E. coli* cells were recovered on the TSA plate (Fig. 7(b)) and the number of colonies was counted.

The results are shown as a graph in Fig. 8. The values of the colonies grown on the plate relative to the positive control (set as %) are about

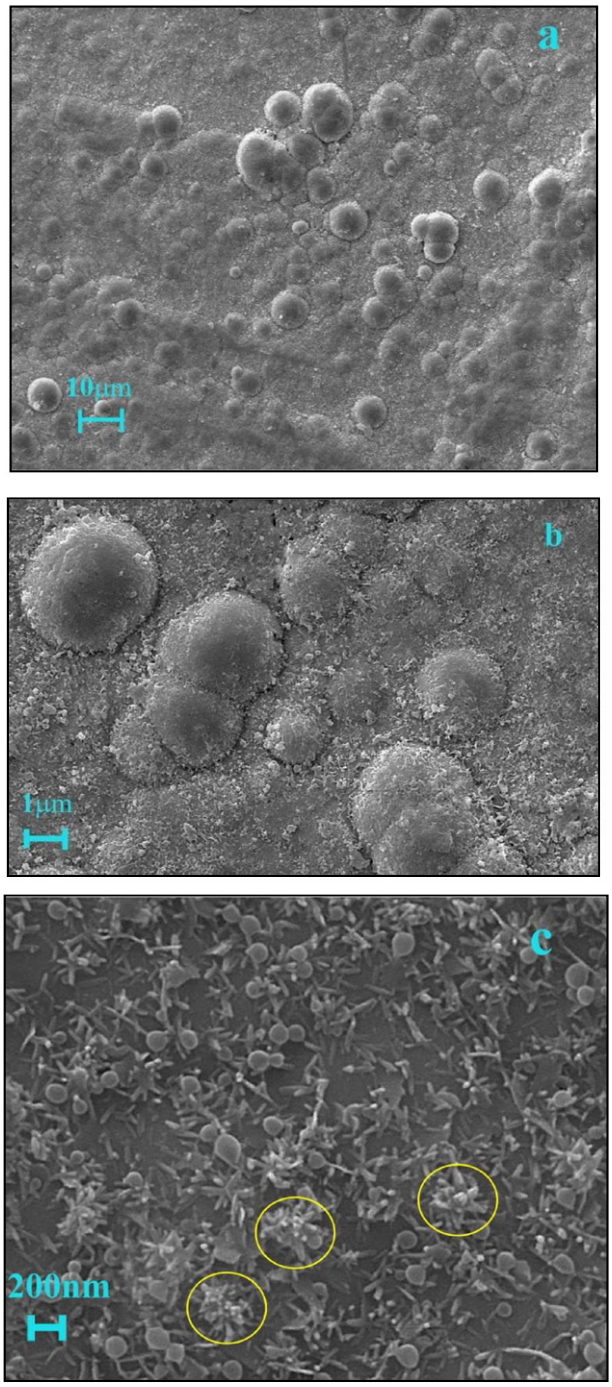


**Fig. 4.** 3D scanning micrographs of the coated surface at different magnifications; (a) 10,000×, (b) 20,000×, and (c) 50,000×.

70% and 5% for the Ni–P coated plate and ZnO NP deposited plate, respectively (the data reported for each specimen is an average of three measurements).

The obtained results could be also expressed as the growth inhibitory percentage by using Eq. (1):

$$\text{Growth inhibitory percentage} = \frac{N_{\text{control}} - N_{\text{sample}}}{N_{\text{control}}} \quad (1)$$

In this equation, $N_{control}$ and $N_{sample}$ correspond to the total CFU of positive control and test plate respectively. The total CFU was calculated from counting of colony number in the TSA agar plates (Fig. 7(b)) with

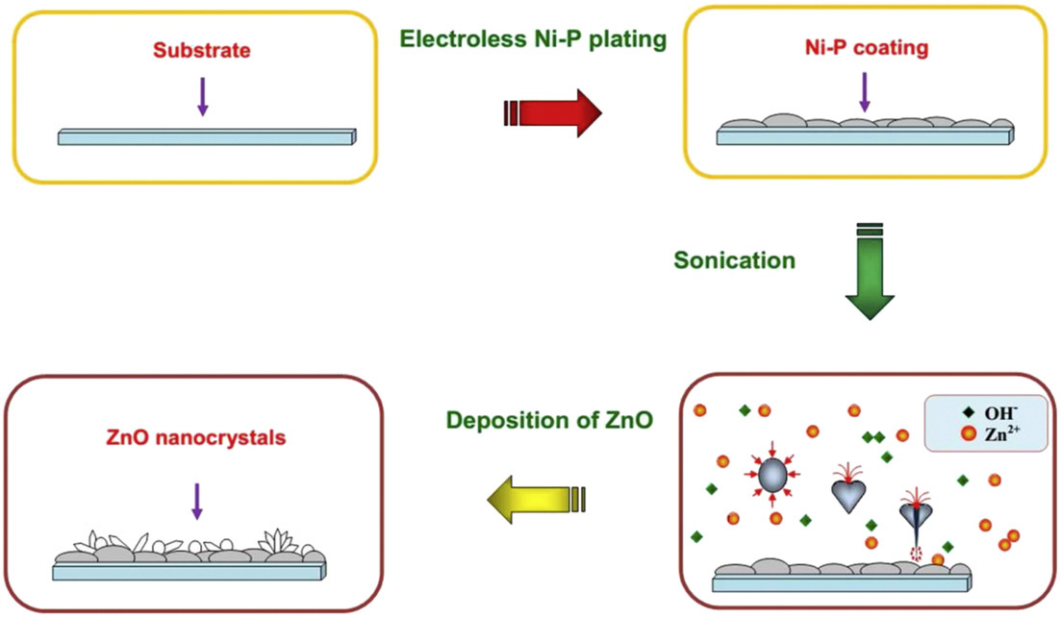


**Fig. 5.** Schematic illustration of the synthesis and deposition of ZnO nanocrystals on the surface in the presence of ultrasonic irradiation. The asymmetric collapse near the surface by the generation of microjets as strong streams results in the particles joining and the formation of the flower-like structure.

regard to the dilution factor. According to Eq. (1), the values of the growth inhibitory percentage for electroless Ni–P plated and ZnO NP deposited surfaces are about 30% and 95%, respectively.

Fig. 9 presents the results of zone of the inhibition test. In the case of the Ni–P coated plates, a significant zone of inhibition was not detected (Fig. 9(a)) whereas a clear inhibition zone was observed in the areas surrounding the surface of ZnO deposited surface (Fig. 9(b)).

It should be mentioned that the Ni–P surface partially showed antibacterial activity by the colony count method. Therefore, based on our results, it can be concluded that the application of the colony count method is more accurate for the determination of the biological activity of the substrate possessing low inherent antibacterial activity.

The reduction of the survival ratio of bacteria (Fig. 8) and the observation of the clean zone surrounding the ZnO attached plate confirm that the target surface has high antibacterial activity against *E. coli*. Indeed, during cultivation, the formation of the active species on the surface and their diffusion to the bacteria suspension may result in killing or growth inhibition of the bacteria. The dominant mechanism for the antimicrobial activity of ZnO was proposed based on the generation of the reactive oxygen species (ROS) such as $OH^-$, $H_2O_2$, and $O_2^-$. The presence of these species in the medium and their penetration in bacterial cells result in the inhibition of cell growth [4,15]. However, the existence of ROS was detected by electron spin resonance (ESR), discovery of the exact mechanism of this generation is still under consideration

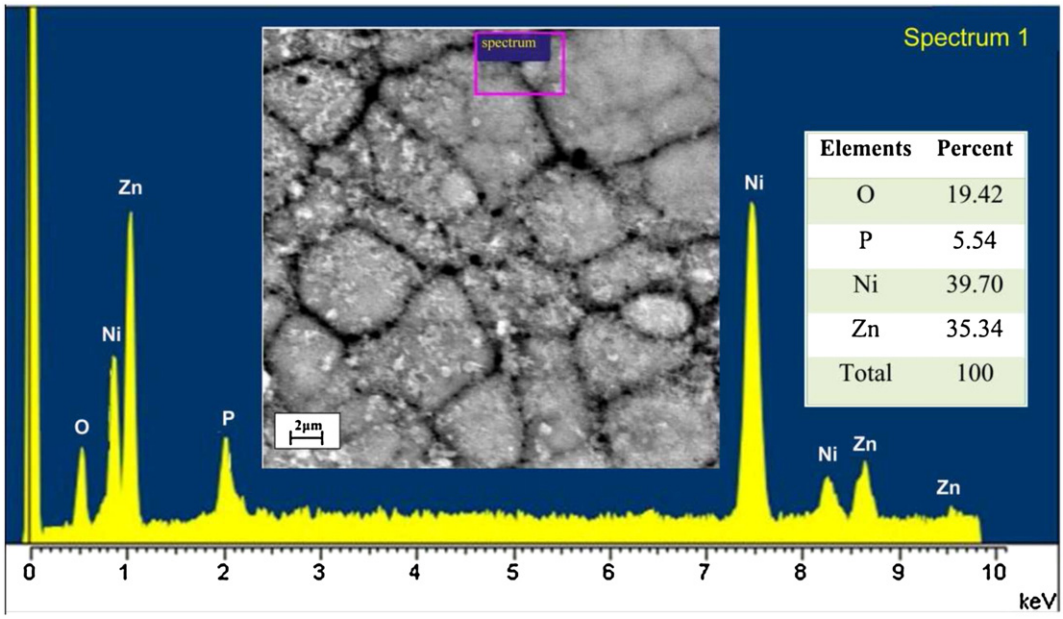


| Elements | Percent |
|---|---|
| O | 19.42 |
| P | 5.54 |
| Ni | 39.70 |
| Zn | 35.34 |
| Total | 100 |

**Fig. 6.** EDX spectrum of the ZnO deposited surface and elemental analysis of the selected region of 2D SEM image from top-view (distinct boundaries which can be seen in this figure are ascribed to the Ni–P layer).

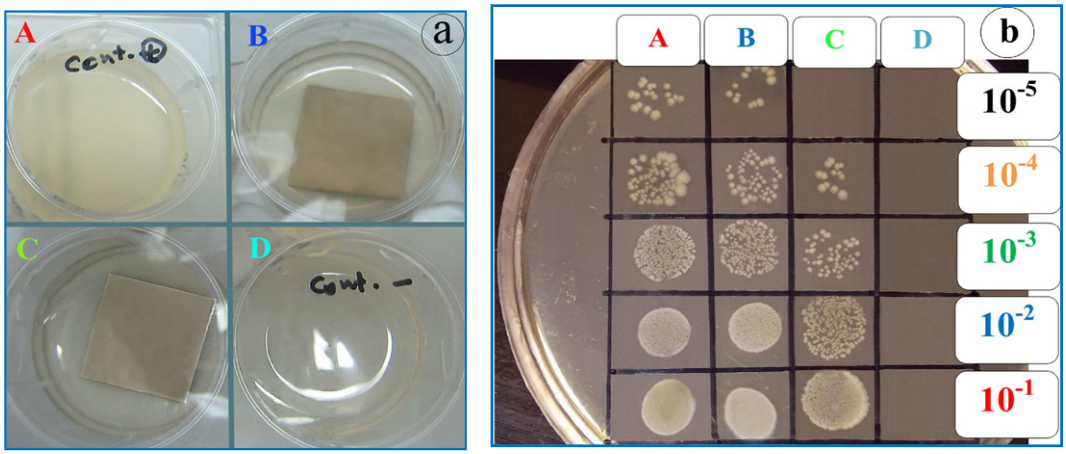


**Fig. 7.** Images of bacteriological test; (a) exposure of the plates to bacterial suspension, (b) recovery of viable *E. coli* cells on solid agar plate for all samples. In both Figures: (A) positive control, (B) Ni–P coated plate, (C) ZnO deposited plate, and (D) negative control.

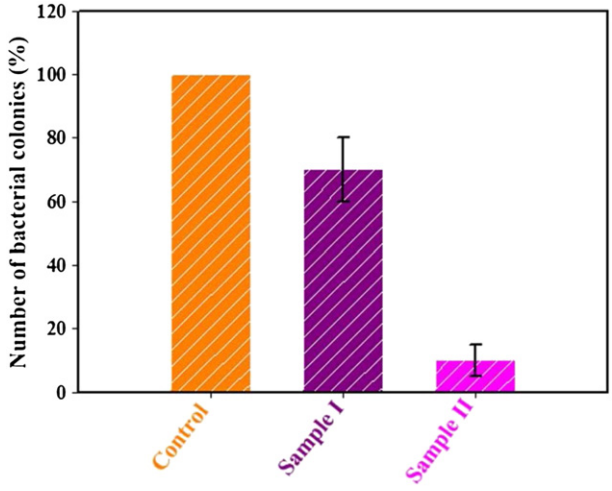


**Fig. 8.** Number of colonies grown on TSA agar plate; samples I and II are attributed to Ni–P coated plate and ZnO deposited surface, respectively.

because this metal oxide indicates antibacterial activity even in the dark [15]. This property of ZnO is also attributed to some other mechanisms like release of zinc ion or internalization of ZnO NPs by the bacterial cell. In this study, the strong linkage between ZnO NPs and the surface arisen from shockwaves have only a minor influence on the dominant mechanism. Moreover, the leaching of Zn ions has a small effect on the antibacterial activity.

In our results, there was also a noticeable point about the role of Ni–P coating in reduction of bacterial growth comparing to the positive control. This could be attributed to the slight dissolving of Ni. It can be assumed that the release of $Ni^{2+}$ from the Ni–P coating and its entry in bacterial cells can lead to a decrease of the bacterial growth. This mechanism has been proved for antibacterial activities of some metals and their alloys such as copper and silver.

## 4. Conclusions

Mild steel was chosen as a suitable metallic surface because of its hardness and strength. Its surface was protected by a Ni–P composite layer. Simultaneous synthesis and deposition of ZnO NPs were successfully carried out on the surface by the sonication method. The morphology and microstructure of ZnO NPs synthesized by ultrasound was compared with ZnO NPs deposited on the surface by TEM and SEM techniques. The biological activity of the target plate was evaluated by colony count method and zone of inhibition test. Our experimental results confirmed that the plate containing ZnO NPs as a rigid antibacterial matrix can reduce the spreading of the secondary pollution and therefore can provide a more sterile environment. Due to the biological activity of Ni–P coating toward *E. coli*, it is highly recommended that more experiments be conducted on the relationship of the grain size and microstructure of this anticorrosive layer to its antibacterial property.

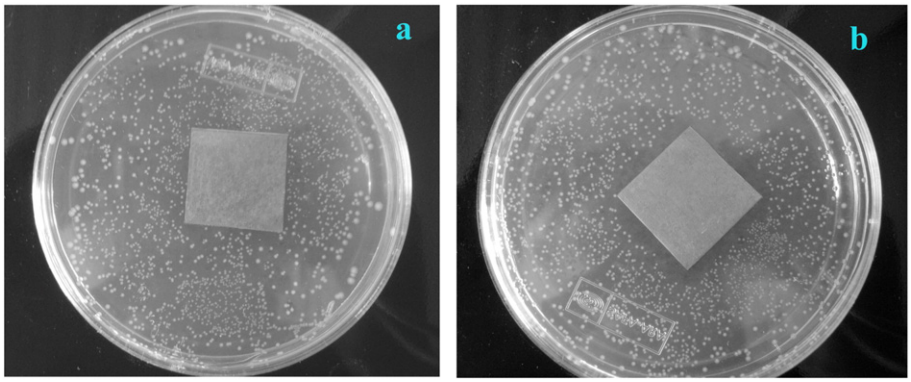


**Fig. 9.** Photographic images of the zone of inhibition test, (a) plate without ZnO and (b) plate with ZnO.

## Acknowledgments

The support of Ferdowsi University of Mashhad (Research and Technology) for this work (code 3/21049, date 08/03/2012) is appreciated.

## References

[1] R. Dastjerdi, M. Montazer, Colloids Surf. B 79 (2010) 5–18.
[2] C.W. Dunnill, K. Page, Z.A. Aiken, S. Noimark, G. Hyett, A. Kafizas, J. Pratten, M. Wilson, I.P. Parkin, J. Photochem. Photobiol. A 220 (2011) 113–123.
[3] L. Budama, B.A. Çakır, Ö. Topel, N. Hoda, Chem. Eng. J. 228 (2013) 489–495.
[4] I. Perelshtein, G. Applerot, N. Perkas, E. Wehrschetz-Sigl, A. Hasmann, G.M. Guebitz, A. Gedanken, Appl. Mater. Interfaces 1 (2009) 361–366.
[5] A. Abramova, A. Gedanken, V. Popov, E.H. Ooi, T.J. Mason, E.M. Joyce, J. Beddow, I. Perelshtein, V. Bayazitov, Mater. Lett. 96 (2013) 121–124.
[6] S. Selvam, R.R. Gandhi, J. Suresh, S. Gowri, S. Ravikumar, M. Sundrarajan, Int. J. Pharm. 434 (2012) 366–374.
[7] G. Applerot, N. Perkas, G. Amirian, O. Girshevitz, A. Gedanken, Appl. Surf. Sci. 256S (2009) S3–S8.
[8] N.C.T. Martins, C.S.R. Freire, C.P. Neto, A.J.D. Silvestre, J. Causio, G. Baldi, P. Sadocco, T. Trindade, Colloids Surf. A 417 (2013) 111–119.
[9] K. Ghule, A.V. Ghule, B.J. Chen, Y.C. Ling, Green Chem. 8 (2006) 1034–1041.
[10] J. Wang, H. Liu, H. Wang, Z. Wang, W. Zhou, H. Liu, Chem. Eng. J. 228 (2013) 272–280.
[11] R. Tankhiwale, S.K. Bajpai, Colloids Surf. B 90 (2012) 16–20.
[12] B. Panea, G. Ripoll, J. González, A. Fernández-Cuello, P. Albertí, J. Food Eng. 123 (2014) 104–112.
[13] A. Esmaeili, M.H. Entezari, J. Colloid Interface Sci. 432 (2014) 19–25.
[14] P. Mishra, R.S. Yadav, A.C. Pandey, Ultrason. Sonochem. 17 (2010) 560–565.
[15] L. Zhang, Y. Jiang, Y. Ding, N. Daskalakis, L. Jeuken, M. Povey, A.J. O'Neill, D.W. York, J. Nanopart. Res. 12 (2010) 1625–1636.
[16] X. Xu, D. Chen, Z. Yi, M. Jiang, L. Wang, Z. Zhou, X. Fan, Y. Wang, D. Hui, Langmuir 29 (2013) 5573–5580.
[17] R.K. Dutta, P.K. Sharma, R. Bhargava, N. Kumar, A.C. Pandey, J. Phys. Chem. B 114 (2010) 5594–5599.
[18] S. Dhoke, A. Khanna, T. Jai Mangal Sinha, Prog. Org. Coat. 64 (2009) 371–382.
[19] A. Kalendova, D. Vesely, Prog. Org. Coat. 4 (2009) 5–19.
[20] X. Wang, L. Zhu, H. Liu, W. Li, Surf. Coat. Technol. 202 (2008) 4210–4217.